Mechanical Systems and Signal Processing 66-67 (2016) 410–424

Contents lists available at ScienceDirect

Mechanical Systems and Signal Processing

journal homepage: www.elsevier.com/locate/ymssp

High performance MEMS accelerometers for concrete SHM applications and comparison with COTS accelerometers

S. Kavitha [a], R. Joseph Daniel [a,*], K. Sumangala [b]

[a] NPMaSS National MEMS Design Centre, Department of Electronics and Instrumentation Engineering, Annamalai University, Annamalainagar 608002, Tamil Nadu, India
[b] Department of Civil and Structural Engineering, Annamalai University, Annamalainagar 608002, Tamil Nadu, India

ARTICLE INFO

Article history:
Received 14 April 2014
Received in revised form
12 December 2014
Accepted 11 June 2015
Available online 2 July 2015

Keywords:
Structural health monitoring (SHM)
MEMS
Piezoresistor
Single axis accelerometer
Cross axis sensitivity
Commercial off-the-shelf (COTS) accelerometer

ABSTRACT

Accelerometers used for civil and huge mechanical structural health monitoring intend to measure the shift in the natural frequency of the monitored structures (< 100 Hz) and such sensors should have large sensitivity and extremely low noise floor. Sensitivity of accelerometers is inversely proportional to the frequency squared. Commercial MEMS (Micro Electro-Mechanical System) accelerometers that are generally designed for large bandwidth (e.g 25 kHz in ADXL150) have poor sensor level sensitivity and therefore uses complex signal conditioning electronics to achieve large sensitivity and low noise floor which in turn results in higher cost. In this work, an attempt has been made to design MEMS capacitive and piezoresistive accelerometers for smaller bandwidth using IntelliSuite and CoventorWare MEMS tools respectively. The various performance metrics have been obtained using simulation experiments and the results show that these sensors have excellent voltage sensitivity, noise performance and high resolution at sensor level and are even superior to commercial MEMS accelerometers.

© 2015 Elsevier Ltd. All rights reserved.

1. Introduction

Structural health monitoring (SHM) has emerged in recent years as an active research area, especially as civil infrastructure systems continue to experience performance degradation due to material aging, improper usage, and various types of hazardous events [1]. A structural health monitoring system collects and analyzes online information about a structure so that indications of structural distress can be identified early. Many types of sensors are commercially available for measuring structural response information that can then be used for diagnosing structural safety conditions [2]. In the recent past, wireless sensors have been considered as a potential alternative to the wired sensors since it offers a more cost effective approach for capturing the acceleration data from the structure.

Even among the wireless sensors being developed, the MEMS acceleration sensors are beginning to play a crucial role since the sensing, signal conditioning and data transmission can be integrated as a single chip. Jerome Peter et al. [2] has conducted extensive research on structural health monitoring, integrating commercial off-the-shelves (COTS) accelerometers for sensing the acceleration and wireless communication equipment for transmission of acquired acceleration data to explore the benefits of wireless structural monitoring systems. In the present scenario, standard practice followed by the

* Corresponding author. Tel.: +91 9445112208 (mobile), +91 4144 239802 (R); fax: +91 4144 238080, +91 4144 238275.
E-mail addresses: kaviraj_2003@rediffmail.com (S. Kavitha), josuma.au@gmail.com (R. Joseph Daniel), josuma@rediffmail.com (K. Sumangala).

http://dx.doi.org/10.1016/j.ymssp.2015.06.005
0888-3270/© 2015 Elsevier Ltd. All rights reserved.

SHM community has been to adapt sensing technologies like MEMS accelerometer to the particular proof-of concept experiment at hand. Micro electro-mechanical systems (MEMS) sensor is fabricated through micro-fabrication techniques and therefore electro-mechanical transduction mechanisms can be combined with micro-circuitry for signal processing and computation [3]. Andreas Vogl et al. [4] reported the design and implementation of a novel wireless MEMS piezoresistive accelerometer sensor with a sensitivity of 0.19 mV/g/V for condition monitoring of AC motors. However, little attention has been paid to the development and implementation of MEMS sensors with the intent of specifically addressing issues related to the concrete SHM application. Such MEMS sensors used for concrete structure health monitoring should be of high sensitivity with ultra low noise floor since most ambient acceleration in civil structures are characterized by low-amplitude acceleration (small g). Secondly, the natural frequencies of civil structures are relatively small and hence the MEMS accelerometers designed for Civil SHM and earthquake sensing need not have larger bandwidth. Ultimately, such sensors should be cheaper and consume less power.

Structural health monitoring using MEMS accelerometers based on different working principles such as piezoresistive, capacitive and piezoelectric have been reported [4,5–8]. However the two dominant microsensor architectures widely considered by researchers are capacitive and piezoresistive. Although both the types of accelerometers employ internal proof masses that are excited by acceleration, the architectural differences are in the transduction mechanism used to correlate the movement of the internal proof mass to acceleration. Capacitive accelerometers employ a differential capacitor whose balance is disrupted by the movement of the proof mass. On the other hand piezoresistive accelerometers generally rely on strain induced within a flexural element that attaches the proof mass to the sensor housing for identification of the mass movement. Capacitive based MEMS accelerometers, such as ADXL series [9] have enjoyed more commercial success than piezoresistive designs [1] due to the problem associated with temperature coefficients, though piezoresistive accelerometers exhibit superior performance in the high frequency bands of interest [2] than capacitive. However, these commercial sensors are designed for general purpose applications and therefore the bandwidth is larger (in the range of 5–20 kHz). Hence such sensors are designed to have a large natural frequency which needs larger stiffness constant (k) and smaller proof mass (m). This ultimately results in poor sensor sensitivity. So the present day MEMS accelerometers largely depend on the signal conditioning electronic circuits for achieving larger sensitivity [10]. But if high sensitivity is achieved in the sensor level itself, it would be desirable. The authors of this present paper have reported the design of MEMS piezoresistive and capacitive accelerometers that satisfy the requirements of accelerometers exclusively meant for concrete SHM applications and earthquake sensing. The main design requirement of accelerometers with an intended application of concrete SHM is high sensitivity to low frequency acceleration. High sensitivity can be achieved with large mass and lower stiffness. But, large mass and lower stiffness will result in lower resonance frequency and hence lower bandwidth (0–100) Hz. However, this is a favorable situation while considering an accelerometer for SHM applications since this application typically needs lower bandwidth. The results of such a design and the displacement analysis, modal analysis, voltage analysis and noise analysis on the designed piezoresistive and capacitive accelerometers were obtained through coventorware and Intellisuite MEMS simulation tools respectively.

A brief survey of the literature [1] indicates that the maximum frequency of the excitation signals used for SHM applications is less than 100 Hz. So the natural frequency of the accelerometers in the present study has been fixed at 100 Hz. Considering the fact that these accelerometers are intended for concrete SHM applications [8], the specifications for accelerometers are chosen as given in the Table 1.

2. Design of MEMS piezoresistive and capacitive and accelerometers for SHM applications

The top view of the MEMS piezoresistive accelerometer considered in this study for concrete SHM applications is shown in Fig. 1a and the cross sectional view along XX[1] of the structure is presented in Fig. 1b. The various silicon processing steps to create this structure for analysis in CoventorWare is presented in Fig. 2. The modern day commercially available capacitive accelerometer such as ADXL series from Analog Devices Inc. [9] use a comb finger type differential capacitive MEMS structure as shown in Fig. 3a. Hence the authors considered the same structure used in ADXL MEMS capacitive accelerometer design in this study that aims at design of high performance MEMS accelerometers for SHM applications.

Table 1
Specifications of the accelerometers for SHM applications.

Parameter	Values
Vibration range	0–2 g
Natural frequency	100 Hz
Displacement sensitivity	24 μm/g
Noise floor	$< 1\mu g/\sqrt{Hz}$
Cross-axis sensitivity	< 1%
Shock resistance	< 500 g

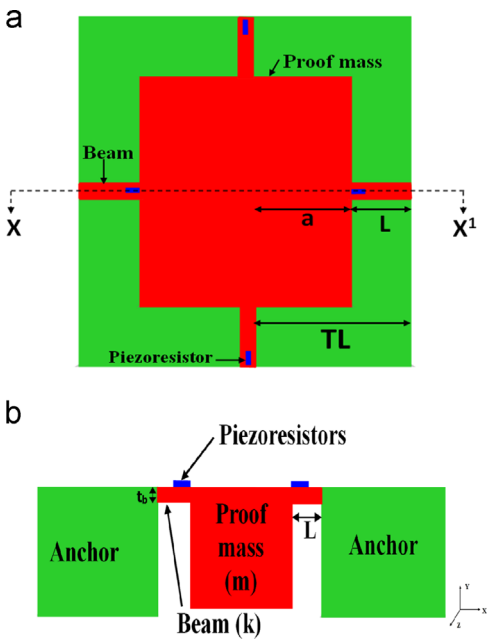

Fig. 1. (a) Top view of the MEMS piezoresistive accelerometer and (b) cross sectional view of the MEMS piezoresistive accelerometer across XX^1.

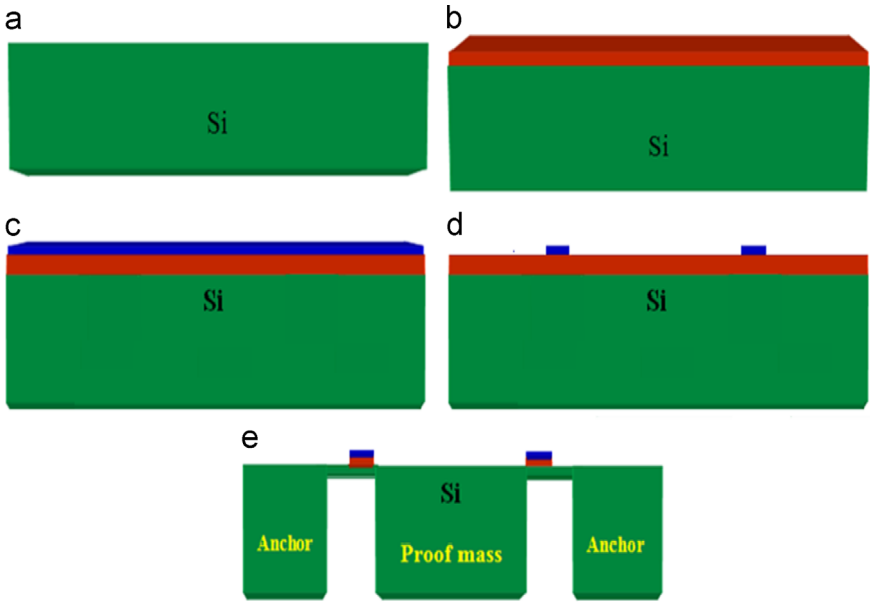

Fig. 2. Silicon processing steps of the piezoresistive accelerometer.

2.1. Design of MEMS piezoresistive accelerometer

The seismic mass (m) is suspended by four symmetrical beams (Fig. 1a and b) that determine the stiffness constant 'k'. This structure with the seismic mass (m) suspended by four symmetrical cantilever beams has been preferred in this study to reduce the cross-axis sensitivity. The other advantage is that this device can be realized using bulk micromachining and hence it paves way for using a large mass which is a typical requirement for achieving higher sensitivity at low frequency ambient acceleration. Four silicon piezoresistors strategically embedded on these four beams gives the stresses caused by acceleration in these beams in terms of change in their resistances. These stresses are the indicator of the ambient accelarations. Therefore, the four piezoresistors organized in a Wheatstone bridge gives the acceleration in z-direction.

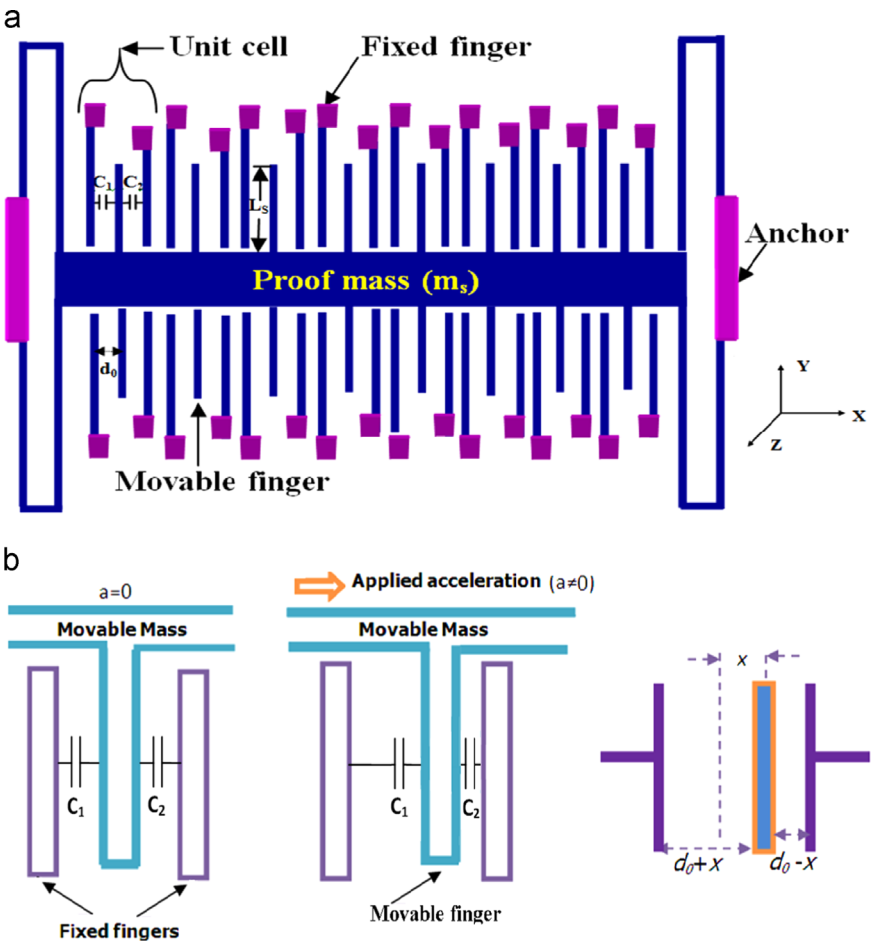

Fig. 3. (a) Structure of MEMS capacitive accelerometer and (b) single unit of differential capacitance in the comb.

The key parameters for the efficient design of an accelerometers are the resonant frequencies, deflection and the stress sensitivities. Hence these parameters are briefly discussed here first.

The resonance frequencies for the several modes of a multiple suspended seismic mass are given by the following equations [4,15,21]:

$$f_{0z} = \frac{1}{2\pi}\sqrt{\frac{k_z}{m}} \tag{1}$$

$$f_{0\theta x} = \frac{1}{2\pi}\sqrt{\frac{k_{\theta x}}{I_{\theta x}}} \tag{2}$$

$$f_{0\theta y} = \frac{1}{2\pi}\sqrt{\frac{k_{\theta y}}{I_{\theta y}}} \tag{3}$$

where f_{0z}, $f_{0\theta x}$ and $f_{0\theta y}$ are the resonant frequencies of the first three modes, $I_{\theta x}$ and $I_{\theta y}$ are the moments of inertia around the x-axis and y-axis respectively, and k_z, $k_{\theta x}$ and $k_{\theta y}$ are the stiffness values of the first three modes which are given by

$$k_z = \frac{4EW_b t_b^3}{L^3} \tag{4}$$

$$\frac{k_{\theta y}}{k_z} = \frac{(L^2 + 3aL + 3a^2)}{6} \tag{5}$$

Table 2
Optimized geometries of piezoresistive accelerometer.

Structural parameters	Dimensions in μm
Proofmass half side length (a)	2600
Proofmass thickness (t_{pm})	860
Beam length (L)	1650
Beam width (W_b)	45
Beam thickness (t_b)	15
Die size	10,000 × 10,000

$$\frac{k_{\theta x}}{k_z} = \frac{(L^2 + 3aL + 3a^2)}{6} \tag{6}$$

where L, W_b, t_b, a and E are the beam length, beam width, beam thickness, proof mass half side length and Young's modulus of silicon respectively. The moment of inertia $I_{\theta x}$ and $I_{\theta y}$ can be obtained as [21]

$$I_{\theta x} = \frac{\rho}{12}\left[(2a)^4 t_{pm} + t_{pm}^3 (2a)^2\right] \tag{7}$$

where ρ and t_{pm} are the density of silicon and proof mass thickness respectively.

The deflection of the proof mass in the Z-axis can be expressed as

$$\delta = \frac{nmgL^3}{48EI} \tag{8}$$

Similarly, the maximum stress can be written as

$$\sigma = \frac{3L}{4W_b t_b^2} mg \tag{9}$$

where n is the acceleration in g (g=9.8 m/s^2), m is the mass of the proof mass and I is the moment of inertia of the beam. The design of the various geometries to meet the specifications listed in Table 1 has been carried out as explained in Kavitha et al. [8]. The various geometries of this designed piezoresistive accelerometer are presented in Table 2.

2.2. Design of MEMS capacitive accelerometer

The capacitive type MEMS accelerometer with the comb drive structure as shown in Fig. 3a has several attractive features. The most important features are their excellent sensitivity and intrinsically insensitive transduction mechanism for temperature, low drift, good noise performance and simplicity [11,12]. Further, capacitive sensing is independent of the base material and relies only on the variation of capacitance when the sensor is subjected to ambient acceleration.

The operations and response of a capacitive accelerometer are controlled by the effective mass of the movable part (m), stiffness constant of suspension beam (k), damping (D) of air surrounding the structure, finger overlap area (A), sensing finger length (L_s), finger initial sensing gap (d_0), initial capacitance (C_0) and finally the applied acceleration (a). Among these parameters, k and m have the most significant impact on the response of the accelerometer. The folded beam, one of the commonly used suspension beam designs of the comb finger type accelerometer holds the mass hanging. There are many movable fingers extruding from the both sides of the proof mass. When the accelerometer is subjected to acceleration, an external force is transferred to the proof mass through the suspension beam. The proof mass together with movable fingers moves along and against the forced direction as shown in Fig. 3b while the fixed combs remain stationary [13]. This movement changes the air gap (d_0) between the fixed fingers and the movable fingers thus changing the capacitances C_1 and C_2 as depicted in Fig. 3b. The overlap area remains constant. This change in capacitances can be measured and calibrated with the applied external acceleration. The movable fingers constitute the differential capacitance pair C_1 and C_2 with left and right comb fingers as shown in Fig. 3b.

When there is no acceleration (a=0), the movable fingers are resting in the middle of the left and right fixed fingers [12]. In this way, the left and right capacitance pairs C_1 and C_2 are equal and can be referred to as C_0 as given in the following equation:

$$C_0 = \frac{\varepsilon_0 \varepsilon_r N_s L_s h}{d_0} \tag{10}$$

where ε_0 is the permittivity constant, ε_r is the dielectric constant of air, h is the height of the finger, d_0 is the air gap between each movable finger and its left and right fixed fingers, N_s is the number of sensing fingers and L_s is the length of the movable or sensing finger. When the acceleration (a) is non-zero, the capacitances C_1 and C_2 are the functions of corresponding displacement x. The proof mass displacement (x) results in due to acceleration [13,14]. The capacitances C_1

and C_2 can be written as [15]

$$C_1 = \frac{\varepsilon_0 \varepsilon_r N_s L_s h}{d_0}\left[1+\frac{x}{d_0}\right] \tag{11}$$

$$C_2 = \frac{\varepsilon_0 \varepsilon_r N_s L_s h}{d_0}\left[1-\frac{x}{d_0}\right] \tag{12}$$

for $x \lll d_0$.

The displacement x must be very small compared to the gap between the fixed and movable fingers (d_0) for ensuring good linearity. If $a \neq 0$ the capacitance of C_1 and C_2 become unequal and the capacitance difference is found by measuring this small displacement (x) and the difference between capacitances C_1 and C_2 is given by

$$\Delta C = C_1 - C_2 = \frac{2\varepsilon_0 \varepsilon_r N_s L_s h}{d_0}\left[\frac{x}{d_0}\right] = 2C_0\left[\frac{x}{d_0}\right] \tag{13}$$

The stiffness constant of two half folded beams can be expressed as [12]

$$k_e = 4k_1 = \frac{4EW_b^3 h}{L_b^3} \tag{14}$$

where k_1 is the stiffness constant of a single half folded beam, W_b is the beam width, k_e is the equivalent stiffness constant and h is the height of the beam. The four half folded beams are connected in parallel and have the same size. The natural frequency f_0 of this spring-mass system as shown in Fig. 3a is given by [12,15]

$$f_0 = \frac{1}{2\pi}\sqrt{K_e/m_s} \tag{15}$$

The deflection sensitivity (S_d) of this device along the sensitive direction can be expressed as

$$S_d = \frac{m_s g}{k_e} = \frac{\rho h[(W_m L_m)+(N_s W_s L_s)]L_b^3}{2EhW_b^3}\ \mathrm{m/g} \tag{16}$$

where ρ is the density of the polysilicon (2.33×10^3 kg/m^3), h is the height of the fingers and mass, W_m is the mass width, L_m is the mass length and N_S, W_S, L_S are the number of sensing fingers, sensing finger width and sensing finger length respectively. The optimized geometries of comb drive type capacitive accelerometer are presented in Table 3.

3. Performance analysis of MEMS accelerometers

Subsequently the designed structures as shown in Figs. 1–3a have been created for the analysis using Coventor and Intellisuite ®CAD MEMS tools respectively. Then the performance evaluation has been achieved by displacement sensitivity analysis, modal analysis, voltage analysis, cross-axis sensitivity analysis and noise analysis using simulation. The details of these performance analyses and the results are presented in this section.

3.1. Deflection sensitivity analysis

The deflection of the central proof mass in the Z-direction in the piezoresistive sensor and the deflection of proof mass along with the moving fingers in it along X-axis in capacitive sensor at various acceleration in the range of 0–2 g have been obtained for both piezoresistive and capacitive comb drive folded beam type MEMS accelerometers using CoventorWare and Intellisuite MEMS CAD tools respectively. The temperature is fixed at 20 °C. The simulation response for deflection study

Table 3
Optimized geometries of comb drive capacitive accelerometer.

Design parameters	Dimensions
Beam width (W_b)	4 μm
Beam length (L_b)	1600 μm
Mass width (W_m)	2000 μm
Mass length (L_m)	5288 μm
Movable finger width (W_f)	4 μm
Movable finger length (L_f)	1000 μm
Fixed finger width (W_{ff})	4 μm
Fixed finger length (L_{ff})	950 μm
Total number of finger (N_f)	4
Device height (h)	4 μm
Capacitance gap (d_0)	250 μm
Anchor size	5172 μm × 20 μm
Air gap between proof mass and substrate	3 μm

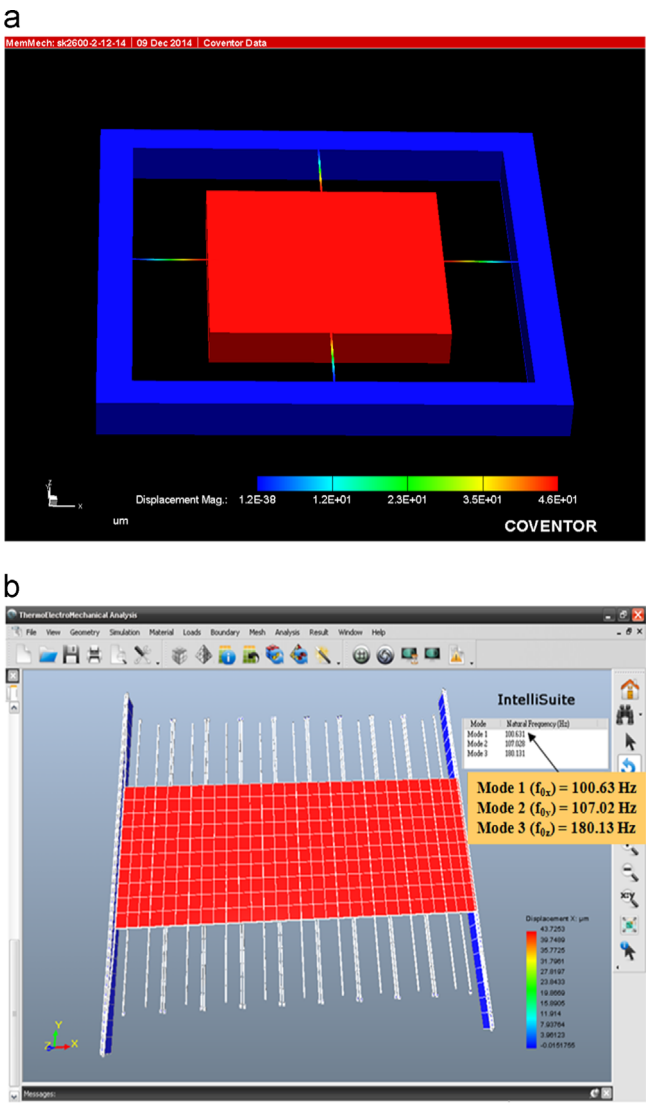

Fig. 4. (a) Deflection analysis of MEMS piezoresistive accelerometer and (b) modal and deflection analyses of MEMS capacitive accelerometer.

for both piezoresistive and capacitive accelerometers are shown in Fig. 4a and b. The deflection versus acceleration graph for both the sensors is shown in Fig. 5 and it gives the measured deflection at various acceleration obtained from simulation experiments. The deflection sensitivity is estimated by finding the slope of the deflection versus acceleration curves. The theoretical deflection is also calculated for both the accelerometers using Eqs. (8) and (16). The deflection sensitivity for both piezoresistive and capacitive accelerometers measured by simulation to be 21.86 μm/g and 23 μm/g respectively and these values closely match the deflection sensitivity of 24 μm/g obtained through theoretical calculation.

3.2. Modal analysis

The acceleration mode analysis for both the MEMS accelerometers were also conducted by CoventorWare and Intellisuite MEMS CAD tools. The first three mode natural frequencies of the piezoresistive accelerometers obtained through the simulation experiments can be seen in Fig. 6a–c and the results are reported in Table 4. The first mode frequencies for both piezoresistive and capacitive accelerometers obtained through simulation are 103.88 Hz and 100.63 Hz respectively against the design value of 100 Hz. Similarly the second and third mode frequencies of piezoresistive accelerometer also closely match with the theoretical values as seen from Table 4. The capacitive accelerometers has also been simulated to get the modal frequency as shown in Fig. 4b and it also matches with the theoretical value closely.

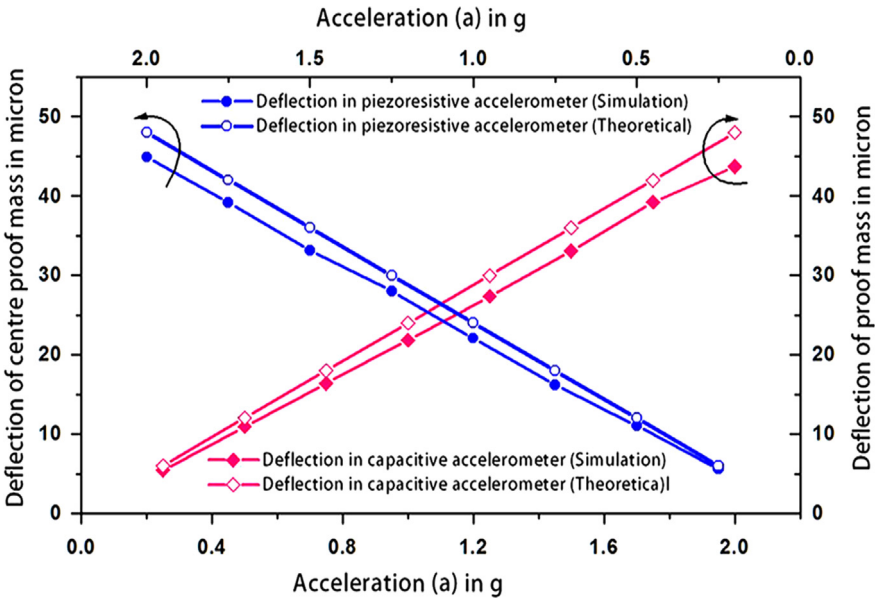

Fig. 5. Deflection versus acceleration graph for both piezoresistive and capacitive accelerometer.

3.3. Cross-axis sensitivity analysis

It is essential that an ideal accelerometer exhibits large linear displacement in the main axis in which the acceleration is measured but nil displacement on the other axes. The present piezoresistive and capacitive accelerometers are intended to measure the acceleration signals in its *Z*-axis (Fig. 7a and b) and *X* and *Z* axes (Fig. 8) respectively. In order to evaluate its cross-axis performance for both the sensors, acceleration was applied in all the directions and the corresponding deflection at various '*g*' are plotted in Fig. 7a, b for piezoresistive accelerometer and Fig. 8 for capacitive accelerometer. It is evident from the Fig. 7a and b, the main axis (*z*-axis) sensitivity is high compared with the other axes sensitivities thus demonstrating the ability of this structure of piezoresistive accelerometer to reduce the cross axis sensitivity. The *X* and *Y* axes sensitivities are 0.92% and 0.90% of main axis sensitivity respectively. These results further show that the piezoresistive accelerometer is a single axis accelerometer.

It is obvious from Fig. 8, the *Y*-axis deflection is three order magnitudes lower than *X*-axis deflection. The *Y*-axis displacement is only 0.193% of the *X*-axis displacement. From this, it is known that this accelerometer has excellent cross-axis performance. However, a displacement proportional to the applied acceleration is measured at *z*-axis and these values are almost equal to the response obtained in *X*-direction. A closer look at the structure of this capacitive accelerometer would show that the *Z*-axis [14] movement is not hindered if it is subjected to a acceleration along this axis. Hence, it can be said that this capacitive accelerometer dealt in this study is a dual axis accelerometer and *z*-axis acceleration could also be measured by this accelerometer.

3.4. Voltage sensitivity analysis

The voltage sensitivity analysis was conducted on both the sensors using simulation. In the pierzoresistive accelerometer, the change in resistance occurs on each piezoresistor due to the applied acceleration. When acceleration is applied, the resistance value of each piezoresistor change due to the piezoresistive effect which in turn changes the Wheatstone bridge output voltage. The bridge output voltage (V_{out}) for 2 g acceleration applied in the *X*, *Y* and *Z*-directions obtained from piezoresistive analysis. The voltage sensitivity for piezoresistive accelerometer is measured to be 3.5634 mV/g/V [8].

The voltage sensitivity of the capacitive accelerometers can be expressed as

$$V_s = \frac{\Delta C}{2C_0} V_m \tag{17}$$

where V_s is the output voltage and V_m is the input modulation voltage. The capacitor C_1 and C_2 at various acceleration levels calculated are used to evaluate ΔC and V_s subsequently using Eq. (13). The output voltage V_s linearly varies with the acceleration in the range of 0–2 g. This linear performance could be achieved since the deflection (δ) at any acceleration is very small compared with d_0. The voltage sensitivity for capacitive accelerometer is measured to be 301 mV/g/V.

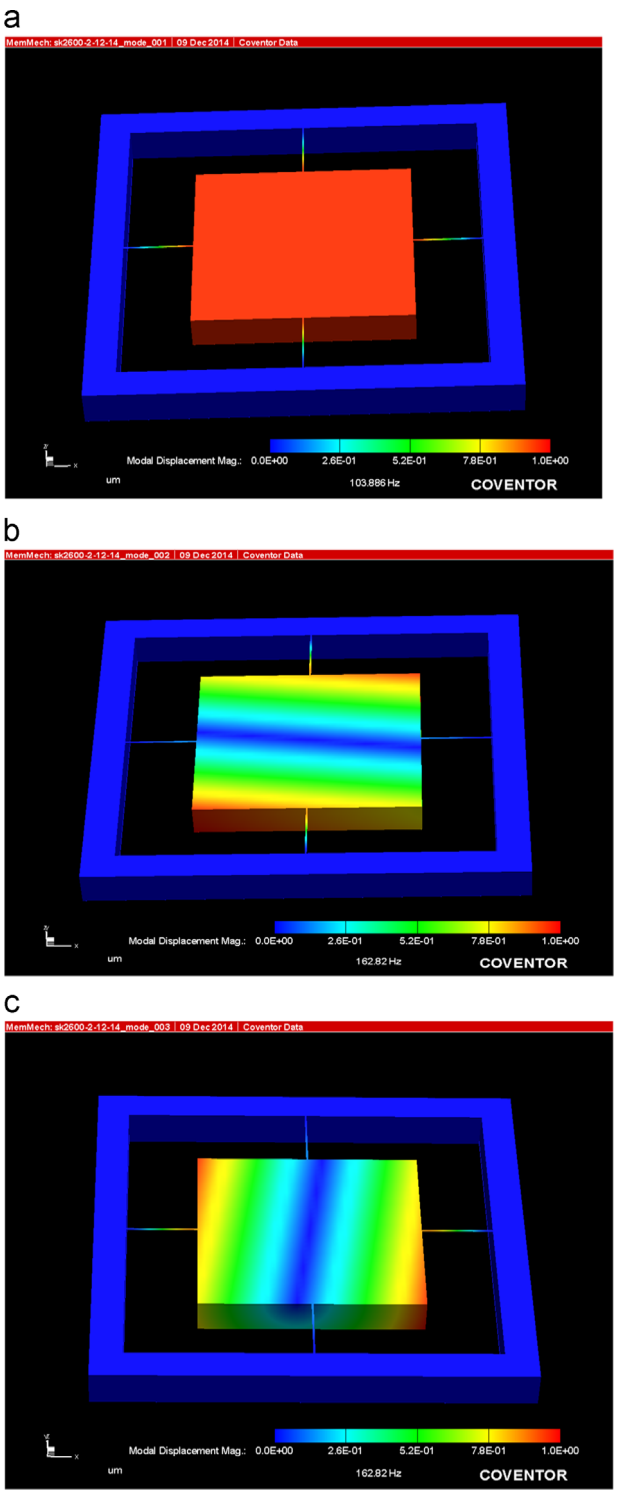

Fig. 6. (a) Modal analysis of MEMS piezoresistive accelerometer (Mode 1), (b) modal analysis of MEMS piezoresistive accelerometer (Mode 2), and (c) modal analysis of MEMS piezoresistive accelerometer (Mode 3).

3.5. Noise analysis and resolution

The main noise sources for this application are expected to be thermal noise (Johnson noise) of the piezoresistors and thermomechanical noise from physical oscillation due to thermal agitation in the sensing structure [16]. The root mean

Table 4
Modal frequency analysis of piezoresistive accelerometer.

$f_{0z}^{(\text{Mode 1})}$ [Hz] Eq. (1)	CoventorWare	$f_{0\theta x}^{(\text{Mode 2})}$ [rads^{-1}] Eq.(2)	CoventorWare	$f_{0\theta y}^{(\text{Mode 3})}$ [rads^{-1}] Eq. (3)	CoventorWare
101.13	103.88	162.52	162.82	162.52	162.82

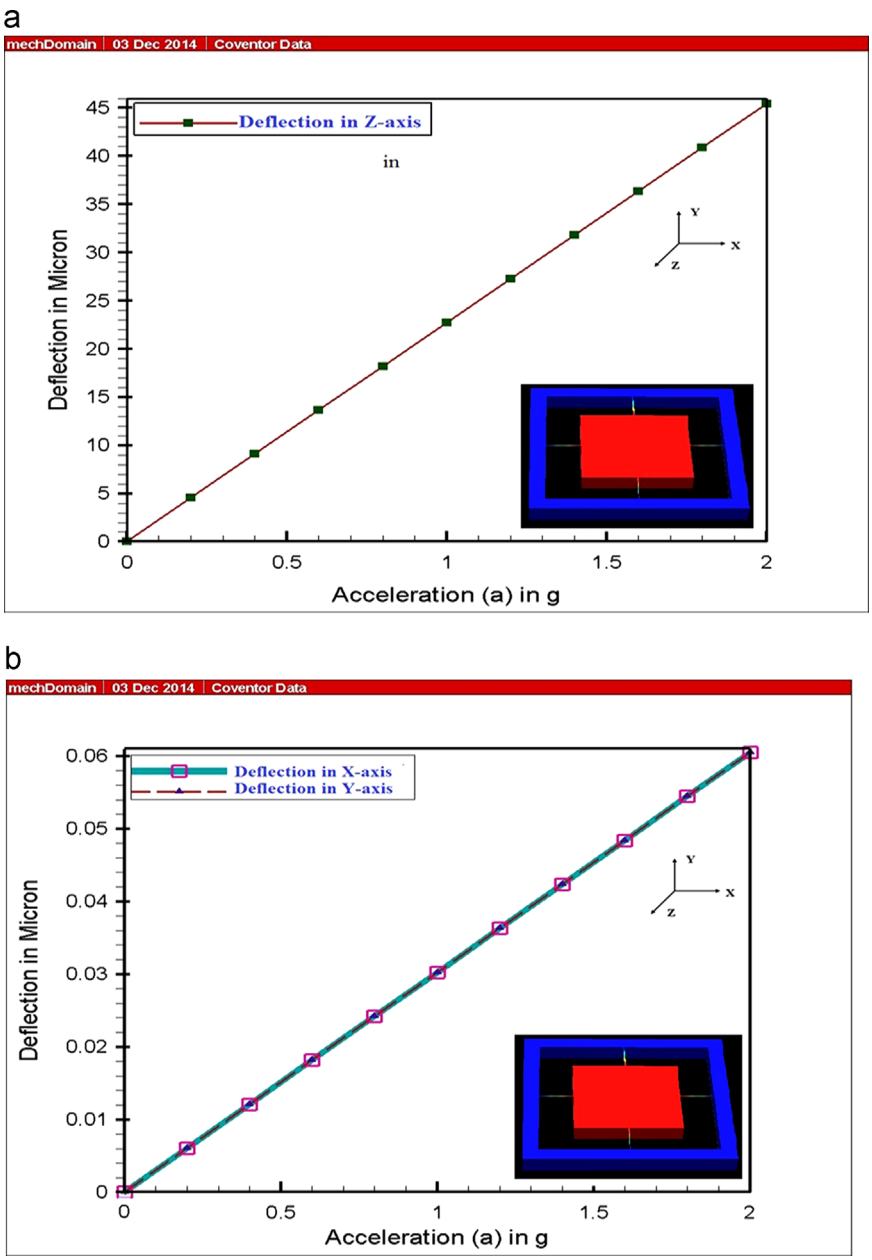

Fig. 7. (a) Cross axis (Z) sensitivity analysis of piezoresistive accelerometer and (b) cross axes (X and Y) sensitivity analysis of piezoresistive accelerometer.

square voltage of equivalent acceleration noise in each piezoresistors is given by

$$V_j = \sqrt{4K_bTR} \quad \text{V}/\sqrt{\text{Hz}} \tag{18}$$

where K_b is the Boltzmann constant, T and R are the temperature of the piezoresistors, the resistance of piezoresistor

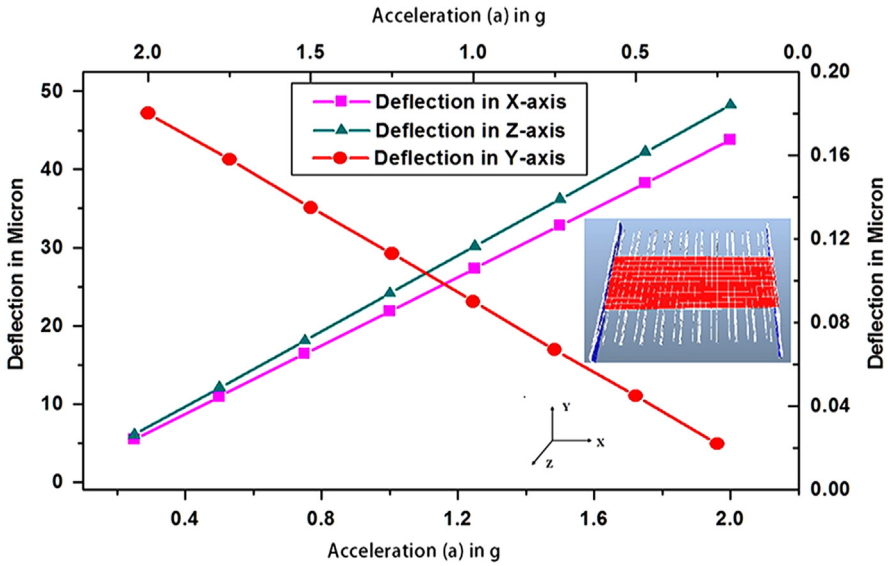

Fig. 8. Cross axis sensitivity analysis of capacitive accelerometer.

respectively. Thermomechanical noise acceleration can be written as [14]

$$x_{tm} = \sqrt{8K_B T\omega_0 \xi/m} \quad \mathrm{g}/\sqrt{\mathrm{Hz}} \tag{19}$$

where m is the mass of the seismic block, ξ is the damping factor. The total noise voltage in the accelerometer is found using the relationship given as [14]

$$V_{nt} = \sqrt{V_j^2 + x_{tm}^2} \quad \mathrm{V}/\sqrt{\mathrm{Hz}} \tag{20}$$

The noise in the piezoresistive accelerometer is estimated to be 4.53 $\mu g/\sqrt{Hz}$. The resolution of an accelerometer determines the minimum acceleration that can be measured. The resolution of piezoresistive accelerometer can be written as [14,15]

$$r = V_{nt}/S_V \tag{21}$$

The resolution is estimated in the piezoresistive accelerometer that is designed to measure a maximum acceleration of 2g and it is calculated to be 12.72 μg. The sensor noise floor in comb drive capacitive accelerometer is usually dominated by the deflection noise, but in mechanical system it is often set by the thermomechanical noise or Brownian noise. The noise arises from the thermal motion of the atoms inside the structure and in the surrounding air and it is a temperature dependent parameter. Thus, the thermal noise displacement for a damped capacitive accelerometer outside the resonance (f_0) is given by [4,15]

$$|x_n(f)| = \sqrt{4k_B T/\omega_o{}^3 m_s Q} \quad \mathrm{m}/\sqrt{\mathrm{Hz}} \tag{22}$$

where k_B is the Boltzmann's constant, m_s is the sensing mass, T is the temperature, ω_0 is the resonance frequency and Q is the quality factor. The estimated noise floor and resolution for capacitive accelerometer are 1.13 $\mu g/\sqrt{Hz}$ and 9.6 μg respectively.

4. Frequency analysis

Accelerometer for concrete SHM need not be designed to sense a broad acceleration frequency range since the concrete structures have a smaller natural frequency. Generally the natural frequency of concrete structures is less than 10 Hz. However, the sensor resonant frequency of Commercial Off-the-shelf sensing technologies (COTS) accelerometer is typically a few kHz (5.5 kHz for ADXL 103/203). Since the sensitivity of a sensor is inversely proportional to sensor bandwidth, COTS accelerometer with larger resonant frequencies will have lower sensitivity and the signal obtained from the sensor is raised to a readable value by a high gain amplifier. The concrete condition monitoring needs less than 100 Hz bandwidth. Hence, it would be better if a acceleration sensor with narrow bandwidth is designed exclusively for concrete SHM applications so that larger sensitivity is obtained from the basic sensing section itself thus reducing the burden of integrating high gain amplifier that follows the sensor. This will in turn reduce the cost. In order to validate this argument, the resonant frequency of the piezoresistive and capacitive accelerometers has been kept at 100 Hz in this design.

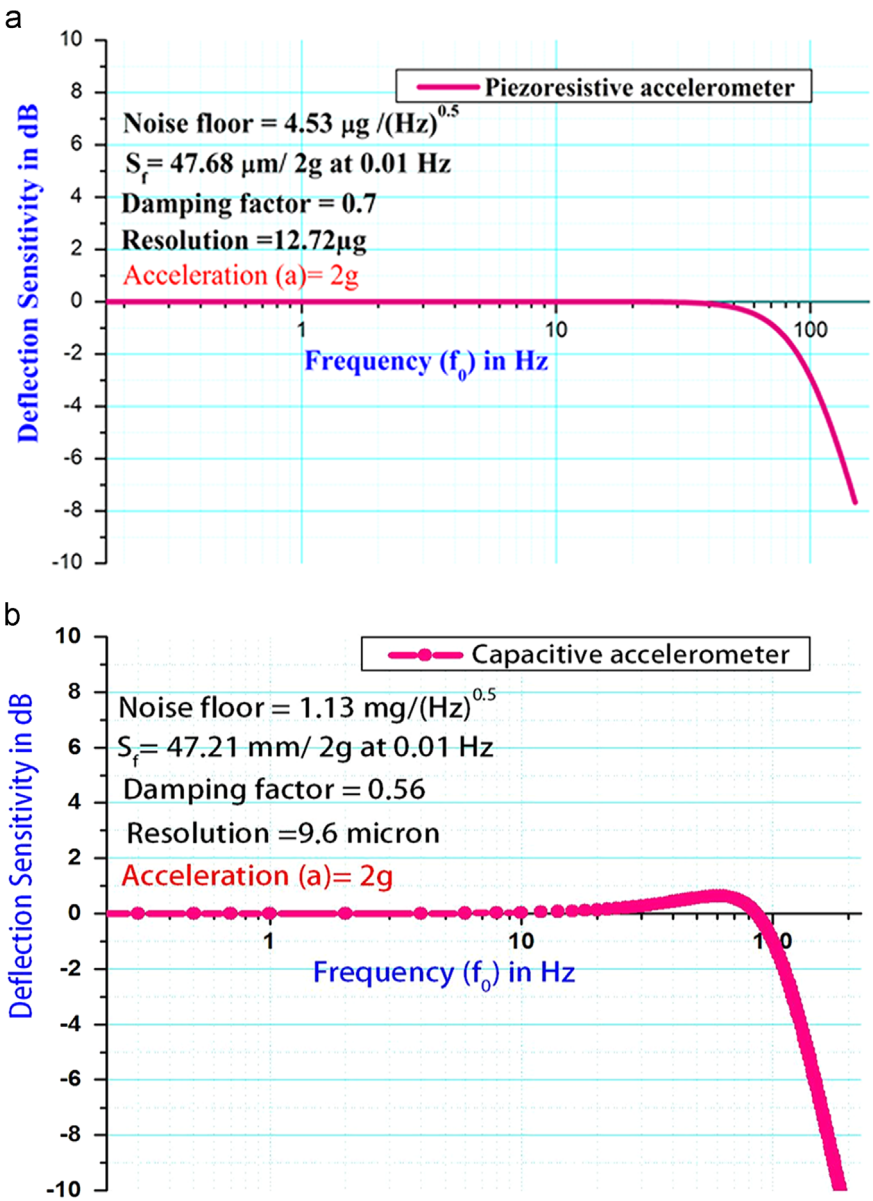

Fig. 9. (a) Deflection sensitivity versus frequency of the piezoresistive accelerometer and (b) deflection sensitivity versus frequency of the capacitive accelerometer.

The simple mass-spring system obeys a second order differential equation given by

$$m\frac{d^2\delta}{dt^2}+b\frac{d\delta}{dt}+k\delta=F(t)=ma \tag{23}$$

where m is the inertial mass, k is the spring constant (N/m), b is the damping coefficient (Ns/m) or the damping factor and a is the acceleration due to external force F. Solving this Eq. (23), the mechanical transfer function from an acceleration to displacement of the mass is obtained as

$$H(s)=\frac{\delta(s)}{a(s)}=\frac{1}{s^2+2\xi\sqrt{k/m}+\frac{k}{m}} \tag{24}$$

The frequency response of this system can be written as

$$\delta=\frac{F/k}{\sqrt{[1-(f^2/f_0^2)]^2+2\xi(f/f_0)^2}} \tag{25}$$

where the $\xi=(b/b_c)$ the ratio of the damping coefficient (b) of the damping medium in the accelerometer to its critical damping coefficient (b_c) [15].

A good design of the piezoresitive accelerometer should aim at an optimal damping factor of 0.7 to achieve maximum bandwidth [17]. Hence the air gap between the proof mass and the top and bottom caps to achieve double sided squeezed film air damping in piezoresistive accelerometer has been designed by setting ξ to be 0.7 in Eqs. (25) where ξ is given as follows:

$$\xi=\frac{4\beta\mu a^2}{h\rho g_0^3\omega_0} \tag{26}$$

where β is the correction factor depending on the geometry of the proof mass ($\beta=0.42$, since the ratio of W/L is 1 for square proof mass) [15,17], g_0, h and μ are the air gap between proof mass and the substrate, height of the proof mass and viscosity of air respectively. The estimated air gap for achieving this damping factor is 50 μm. The frequency response characteristics of the piezoresistive accelerometer were obtained using Eq. (25) and it is plotted as shown in Fig. 9a.

The damping ratio for capacitive accelerometer can be calculated from the lumped damping coefficient b using [15]

$$\xi=\frac{b}{4\pi f_r m_s} \tag{27}$$

The lumped damping coefficient for one pair of finger surfaces or a unit cell can be expressed as [18]

$$b=\frac{\eta A_{fingersurface}}{d_0}+\frac{\eta A_{proofmass}}{g_0} \tag{28}$$

where η is the viscosity of air (2×10^{-5} Pa s), d_0 is the air gap between the fixed and moving fingers at no acceleration, g_0 is the air gap between the proof mass and the substrate, $A_{proof\ mass}$ is the length (L_m) multiplied by width (W_m) of the proof mass and $A_{fingersurface}$ is the length (L_s) multiplied by the height (h) of the movable fingers. The damping ratio (ξ) for this device is calculated to be $\xi=0.56$.

The frequency response characteristics of the capacitive accelerometer were obtained using Eqs. (27), (28) and (29) as shown in Fig. 9b. The applied acceleration has been kept at $2g$ and the sensitivity in dB has been obtained using the relationship

$$S_d=20\log(S_d/S_f)\ \text{dB} \tag{29}$$

where S_d is the deflection sensitivity at any given frequency and S_f is the sensitivity at a reference frequency that is kept as 0.01 Hz in this calculation. The response shows that the sensor ensures linear behaviors in 0–20 Hz range. Hence it satisfies the requirement of a low frequency acceleration sensor for SHM and seismic applications.

5. Comparison of performances with COTS accelerometers and discussions

In order to make the comparison simpler, the various performance metrics such as voltage sensitivity, flat frequency bandwidth and resolution for both the sensors have been summarized in Table 5 along with the same parameters measured by Acar et al. [19,20] for certain COTS accelerometers. It is observed from Table 5, that the capacitive type comb drive folded beam type accelerometer has excellent voltage sensitivity (301 mV/g/V), very low noise floor (1.12 μg/$\sqrt{}$Hz EMBEDhigheration.3) and high resolution than other sensors.

6. Reliability of the CAD simulation results

It is always a question if it is possible to realize the structure with the performance estimated through FEM simulations. The sensitivity is inversely proportional the first resonant frequency squared in an accelerometer. So the measure of the resonant frequency of the physically realized structure is a real indicator of accuracy. Andreas Vogl et al. [4] had fabricated

Table 5
Comparison of performances of present sensors with measured performance of COTS accelerometer by Acar et al. [19,20].

Device/manufacturer	Range (g)	Measured sensitivity	Flat frequency response range (Hz)	DC-100 Hz, 0–2g resolution (μg)	Amplifying electronics
7290A-10 (Endevco)	0–2	199.9 mV/g	1–200	84	Yes
ADXL210A (Analog Devices)	0–10	108.0 mV/g	1–16	258	Yes
M1220D (Motorola)	0–8	241.4 mV/g	1–90	1237	Yes
Silicon Design (SD2012-10)	0–10	399.3 mV/g	1–200	124	Yes
Jerome [1]	0–10	1.25 mV/g	0–680	20	No
Piezoresistive accelerometer (present paper)	0–2	4 mV/g/V	0–45	12.72	No
Capacitive accelerometer (present paper)	0–2	301 mV/g/V	0–30	9.6	No

an piezoresistive accelerometer with the identical structure and measured its performance. The sensor reported in their work gave the first mode frequency as 8 kHz in the simulations. The measured first mode frequency of the fabricated device was 7.7 kHz thus indicating small deviation from CAD results. When the beam thickness was increased to achieve the specified resonant frequency of 10 kHz, the simulated frequency was 10.36 kHz and the measured frequency the fabricated device was 10.3 kHz. The spread in the natural frequency was due to variations of the oscillating mass and beam thickness caused by processing non-uniformity across the wafer as seen from the SEM photograph. The average resonance frequency did not change considerably after glass encapsulation, indicating that the wafer bonding does not introduce significant tensile nor compressive stress in the beams. Hence, minor difference can be expected between the computational and measured parameters. Similarly the performance will be closer to the anticipated results in the present sensor also since the geometries of the present sensor are considerably larger and therefore it is possible to precisely micromachine this structure with the present day technologies.

7. Conclusions

Structural health monitoring of civil structures requires the measurement of acceleration signals that are low in magnitude and frequency. The commercially available MEMS accelerometers have been designed for general purpose use and therefore generally have larger bandwidth. So the natural frequencies (f_0) of these sensors are high. But the deflection sensitivity is inversely proportional to the square of natural frequency. Therefore, the displacement sensitivity of such sensors is relatively low and these do not ensure accurate measurement of acceleration signals from huge civil structures. The sensitivity can be considerably improved by designing the accelerometer for low natural frequency which is an essential requirement for SHM application.

(i) The performance analysis of piezoresistive and capacitive accelerometers results showed that the comb drive folded beam type capacitive accelerometer has excellent voltage sensitivity (301 mV/g/V), very low noise floor (1.13 $\mu g/\sqrt{Hz}$) and high resolution (9.61 μg).
(ii) The designed piezoresistive accelerometer for SHM applications has a voltage sensitivity of 4 mV /g/V, noise floor (4.53 $\mu g/\sqrt{Hz}$) and resolution of (12.72 μg).
(iii) The comparison results clearly bring out the superior performance of MEMS comb drive accelerometer and piezoresistive accelerometer compared with COTS accelerometers. It is further important to note that the displacement sensitivity is considerably higher than the values reported in the literature thus justifying the need to exclusively design and fabricate accelerometers for SHM and seismic applications. Above all, the surface micro-machined comb drive silicon capacitive accelerometer presented in this work is the first of its kind for low *g* and low frequency applications to the authors' knowledge.

Acknowledgment

The authors acknowledge the support received from National Program on Micro and Smart Systems (NPMaSS) and financial support from University Grants Commission (UGC), UGC Reference no.: F.37-49/2009, New Delhi, India through MRP (Major Research Project) scheme. Also the authors record their sincere gratitude to the reviewer for his useful suggestions that has improved the quality of the present paper significantly.

References

[1] Jerome P. Lynch, Aaron Partridge, Kincho H. Law, W. Thomas, W. Kenny, Anne S. Kiremidjian, Ed Carryer, Design of piezoresistive MEMS based accelerometer for integration with wireless sensing unit for structural monitoring, J. Aerosp. Eng. 16 (2003) 108–114.
[2] Jerome P. Lynch, Yang Wang, Kennth J. Loh, Jun Yi, Chung-Bang Yun, Wireless structural monitoring of the geumdang bridge using resolution enhancing signal conditioning, in: Proceedings of the 24th International Modal Analysis Conference (IMAC XXIV), St. Louis, MO, January 30–February 2, 2006.
[3] Takeshi Miyashita, Masatsugu Nagai, Vibration-based structural health monitoring for bridges using laser doppler vibrometers and MEMS-based technologies, Steel Struct. 8 (2008) 325–331.
[4] Andreas Vogl, Dag T Wanga, Preben Storasa, Thor Bakkea, Maaike, M.V. Taklo, Allan Thomson, Balgard Lennart, Design, process and characterisation of a high-performance vibration sensor for wireless condition monitoring, Sens. Actuators A 153 (2009) 155–161.
[5] S. Kavitha, R. Joseph Daniel, K. Sumangala, Computer modelling, design and analysis of piezoresistive MEMS accelerometer for concrete SHM applications, in: Proceedings of Seventh Structural Engineering Convention, vol. I, Allied Publishers Pvt. Ltd., India, 2010, pp. 367–376.
[6] S. Kavitha, R. Joseph Daniel, K. Sumangala, Design and analysis of bulk micromachined piezoresistive MEMS accelerometer for concrete SHM applications, in: Proceedings of the ISSS International Conference on Smart Materials, Structures and Systems, Bangalore, India, January 04–07, 2012.
[7] S. Kavitha, R. Joseph Daniel, K. Sumangala., Computer aided design and effects of beam placement on bulk micromachined piezoresistive MEMS accelerometer for concrete SHM applications, in: Proceedings of the International Conference on Soft Computing and Modeling, Procedia Engineering, Nagercoil, India, 2012.
[8] S. Kavitha, R. Joseph Daniel, K. Sumangala, A simple analytical design approach based on computer aided analysis of bulk micromachined piezoresistive MEMS accelerometer for concrete SHM applications, J. Measure 46 (2013) 3372–3388.
[9] ADXL 150/250, Specification Data Sheets, Analog Devices Inc., 1998.
[10] R.O. Curadelli, J.D. Riera, D. Ambrosini, G. Amani, Damage detection by means of structural damping identification, Eng. Struct. 30 (2008) 3497–3504.

[11] Robert G. Walmsley, Lennie K. Kiyama, Don M. Milligan, Rod L. Alley, David L. Erickson, Peter G. Hartwell, Micro-G, silicon accelerometer using surface electrodes,in: Proceedings of IEEE SENSORS, Conference, 2009.
[12] Wai-chi, W. Azid., B.Y. Majlis, Formulation of stiffness constant and effective mass or a folded beam, Arch. Mech. 62 (2010) 405–418.
[13] E. Ismail, Gonenil, Zeynep Celik-Butler, P. Donald, Surface micromachined MEMS accelerometer on flexible polymide substrate, IEEE Sens. J. 11 (2011).
[14] O. Sidek, M. Afif, M.A. Miskam, Design and simulation of SOI-MEMS *z*-axis capacitive accelerometer, Int. J. Eng. Technol. 10 (2010) 7–13.
[15] M.H. Bao, Micro Mechanical Transducers, Pressure sensors, Accelerometers an Gyroscopes, Handbook of Sensors and Actuators, Elsevier, Amsterdam, 2000.
[16] Dyung Viet Dao, Toshiyuki Toriyama, Susumu Sugiyama., Noise and Frequency Analysis of a Miniaturized 3-DOF Accelerometer Utilizing Silicon Nanowire Piezoresistors, IEEE, 2004.
[17] Minhang Bao, Heng Yang, Squeeze film air damping in MEMS, Sens. Actuators A 136 (2007) 3–27.
[18] G.K. Ananthasuresh, K.J. Vinoy, K.N. Bhat, Micro and Smart Systems, Wiley Publishers, New Delhi, India, 2010.
[19] Cenk Acar, Andrei M. Shkel, Experimental evaluation and comparative analysis of commercial variable-capacitance MEMS accelerometers, J. Micromech. Microeng. 13 (2003) 634–645.
[20] C. Acar, A.M. Shkel, Comparative Characterization of Low-g Capacitive MEMS Accelerometers, Structural Health Monitoring from Diagnostics and Prognostics to Structural Health Management, DEstech Publications, USA, 2003, pp. 1059–1066.
[21] R.P. van Kampen, R.F. Wolffenbuttel, Modeling the mechanical behavior of bulk-micromachined silicon accelerometers, Sens. Actuators A 64 (1998) 137–150.